HHS Public Access

Author manuscript

Sci Signal. Author manuscript; available in PMC 2023 February 27.

Published in final edited form as:

Sci Signal. 2023 January 03; 16(766): eadd3269. doi:10.1126/scisignal.add3269.

Neurodevelopmental disorder-associated mutations in TAOK1 reveal its function as a plasma membrane remodeling kinase

Neal Beeman[1], **Tanmay Sapre**[1], **Shao-En Ong**[1], **Smita Yadav**[1,*]

[1]Department of Pharmacology, University of Washington, Seattle WA 98195

Abstract

Mutations in *TAOK1,* which encodes a serine-threonine kinase, are associated with both autism spectrum disorder (ASD) and neurodevelopmental delay (NDD). Here, we investigated the molecular function of this evolutionarily conserved kinase and the mechanisms through which *TAOK1* mutations may lead to neuropathology. We found that TAOK1 was abundant in neurons in the mammalian brain and remodeled the neuronal plasma membrane through direct association with phosphoinositides. Our characterization of four NDD-associated *TAOK1* mutations revealed that these mutants were catalytically inactive and were aberrantly trapped in a membrane-bound state, which induced abnormal membrane protrusions. Expression of these TAOK1 mutants in cultured mouse hippocampal neurons led to abnormal growth of the dendritic arbor. The coiled-coil region C-terminal to the kinase domain was predicted to fold into a triple helix, and this region directly bound phospholipids and was required for both membrane association and induction of aberrant protrusions. Autophosphorylation of Thr^{440} and Thr^{443} in the triple helix region by the kinase domain blocked the plasma membrane association of TAOK1. These findings define TAOK1 as a plasma membrane remodeling kinase and reveal the underlying mechanisms through which TAOK1 dysfunction may lead to neurodevelopmental disorders.

INTRODUCTION

Neuronal morphogenesis, migration, and maturation rely on extensive remodeling of the neuronal plasma membrane. In addition to the well-appreciated role of the microtubule and actin cytoskeleton in regulating plasma membrane shape and dynamics, proteins can directly associate with the cell membrane through electrostatic interactions to deform and shape membrane (1). Membrane remodeling proteins identified to date belong to the Bin/Amphiphysin/Rvs (BAR) superfamily, in which member proteins consist of a membrane-associating BAR domain. The BAR domain is structurally defined as an elongated

*Corresponding author: smitay@uw.edu.

AUTHOR CONTRIBUTIONS: N.B. performed all but the mass spectrometry experiments. N.B. and S.Y. analyzed the data. T.S. performed mass spectrometry experiments and analyzed the data. S.-E.O. supervised the mass spectrometry and data analyses. S.Y. designed and supervised all experiments, obtained funding, and wrote the manuscript.

Supplementary Materials
Figures S1 – S4

Competing interests: The authors declare that they have no financial or commercial conflicts of interest.

Data and Materials Availability: All data needed to evaluate the conclusions in the paper are present in the paper or the Supplementary Materials. All materials generated in this study will be shared upon request.

homodimer with a shallow curved surface formed by the antiparallel interaction of two triple helix coiled-coils (2–5). This curved BAR dimer interacts with cellular membranes and causes membrane deformation (6). Depending on whether the concave or convex surface of the BAR dimer binds membranes, either membrane invagination or outward protrusions are generated (3, 7, 8). To date, membrane remodeling proteins outside the BAR domain family have not been identified. In this study, we found that an autism risk gene, *TAOK1*, encodes a unique protein kinase that can remodel the plasma membrane by direct binding with phospholipids in an activity-dependent manner.

Thousand and one amino acid kinase 1 (TAOK1) is an evolutionarily conserved serine-threonine kinase (9, 10). Several missense and truncation mutations in *TAOK1* have been identified in patients with severe neurodevelopmental delay (NDD) (11–15). The core clinical features of patients with TAOK1-associated NDD syndrome include varying degrees of intellectual disability and developmental delay, neonatal feeding difficulties, overlapping dysmorphic facial features, behavior problems, hypotonia, and joint hypermobility (11–13). Although evidence for these associations of TAOK1 is compelling, little is known about the molecular and cellular function of TAOK1 in neuronal development. Knockdown of TAOK1 *in utero* in mice causes defects in neuronal migration, and its overexpression leads to dendritic arborization defects (11). TAOK1 is phosphorylated by the Hippo-pathway kinase MST3, which is important for dendritic spine formation (16). In *D. melanogaster*, activity of homolog dTao is required for neuroblast proliferation and neuronal connectivity (17–19). Kin-18 is a homolog of Tao kinases in *C. elegans* that is important for development of embryonic polarity (20). Despite its role in diverse aspects of neuronal development and its strong association with neurodevelopmental disorders, the molecular function of TAOK1 is unknown. Further, how mutations associated with NDD impact TAOK1 function and contribute to neuropathology remains unknown.

Through the study of ASD-associated mutations in TAOK1, we found thatTAOK1 is a plasma membrane remodeling kinase. We found that it binds phosphoinositides and induces plasma membrane protrusions in an activity-dependent manner. Catalytically dead NDD-associated mutations in TAOK1 disrupt its kinase function-dependent autoregulation, resulting in its constitutive membrane binding that leads to aberrant neuronal membrane protrusions and dendritic growth defects in hippocampal neurons. By delineating how TAOK1 controls its membrane association, our results provide evidence for a previously unappreciated regulatory mechanism for membrane remodeling that is important for neuronal morphogenesis, the dysfunction of which may contribute to neuropathology in autism and neurodevelopmental delay.

RESULTS

TAOK1 is highly expressed in neurons in the mammalian brain

TAOK1 is a large protein of 1001 amino acids that comprises an N-terminal kinase domain followed by predicted coiled-coil domains of unknown function. Both the kinase domain and the coiled-coils are structurally conserved across worm, fly, fish, rodent and human species (Fig. 1A). We first investigated expression level of *TAOK1* mRNA in the brain in both human and rodents by analyzing transcriptome databases (21–23). In humans, *TAOK1* is

highly expressed in the prenatal and postnatal stages of brain development, and in the adult human across brain regions, including the neocortex, hippocampus, cerebellum, amygdala and striatum (fig. S1A–E). At the protein level, TAOK1 was the highest in neuronal cell types in both human cortex and hippocampus, with low amounts detected in non-neuronal cells (fig. S1F). Similarly, *Taok1* mRNA was widely expressed in all brain regions in the mouse brain. Cortical layer 2/3, the pyramidal layer hippocampal CA1, granular layer CA3 and DG and cerebellum exhibited the highest expression by *in situ* hybridization (Fig. 1B). Using antibodies against TAOK1 protein, we found that TAOK1 was expressed at a higher level in hippocampal neurons compared to non-neuronal cells and was localized throughout the soma, dendrites and axons (Fig. 1C–D). Next, we generated a GFP-tagged TAOK1 construct, which upon expression in hippocampal neurons was localized similarly to the endogenous TAOK1 protein and was present in all neuronal subcompartments (Fig. 1D).

Several NDD-associated mutations in TAOK1 kinase domain are catalytically deficient and lead to plasma membrane protrusions

We next investigated the impact of ASD- and NDD-associated mutations on TAOK1. These mutations are spread out across the length of the protein encoded by *TAOK1* (fig. S2A). TAOK1 is predicted to be extremely intolerant of mutations (data from gnomAD browser), with a pLI score (24, 25) of 0.998 and a ratio of the observed/expected variants (as determined by O/E constraint score) of 0.17. Of the 28 NDD-associated mutations identified to date within TAOK1, we focused on four mutations that are clustered within its catalytic domain (fig. S2A and Fig. 2A). We performed in vitro kinase assays to determine the impact of these mutations on the enzymatic activity of TAOK1. TAOK1 autophosphorylates itself at the Ser^{181} residue in the catalytic loop, which can be used as a measure of its kinase activity (26). HEK293T cells were transfected with GFP-tagged wild-type or mutant TAOK1, and immunoprecipitated TAOK1 was then subjected to in vitro kinase assay. Probing with an antibody that recognizes the phosphorylated Ser^{181} residue, we found that wild-type TAOK1 showed robust kinase activity; however, all four NDD-associated TAOK1 mutants—S111F, L167R, A219V and R269Q—were catalytically “dead” (Fig. 2B–C). Next, we expressed GFP-tagged TAOK1 constructs harboring the NDD-associated kinase-deficient mutations in HEK293T cells. Whereas wild-type (WT) TAOK1 appeared primarily cytosolic, the kinase-deficient disease-associated mutants were enriched at the plasma membrane (Fig. 2D–E and fig. S2B). Concomitant with their plasma membrane localization, all four NDD-associated kinase-deficient TAOK1 constructs led to aberrant and exuberant protrusions of the plasma membrane, whereas expression of the wild-type TAOK1 did not promote membrane protrusions (Fig 2D and fig. S2B–C).

NDD-associated mutations in TAOK1 cause defects in dendrite development

To test the functional impact of these mutations on neuronal development, we expressed wild-type TAOK1 and ASD mutant TAOK1 in hippocampal neurons. Neurons were transfected at DIV9 and then fixed at DIV11 to determine the impact of these mutations on dendritic growth. Expression of the catalytically dead NDD-associated TAOK1 mutants severely perturbed neuronal development compared to WT TAOK1 (Fig. 2F–H, and fig. S2D). Similar to observations in HEK293T cells, the catalytically dead TAOK1 mutants localized to the plasma membrane and induced abnormal protrusions that were most

apparent within the soma of the hippocampal neurons (Fig. 2F and fig. S2D). The number of secondary and tertiary dendrites were significantly reduced on expression of the four kinase-dead mutants (Fig. 2G). Further, total dendrite length of both primary dendrites and secondary or tertiary dendrites was significantly decreased in neurons expressing the TAOK1 mutants, as opposed to the WT TAOK1 (Fig. 2H).

TAOK1 coiled-coil helical bundle is necessary and sufficient for plasma membrane tubulation

We tested whether acute inhibition of the wild-type TAOK1 through kinase inhibitors would recapitulate plasma membrane binding phenotype of kinase-dead TAOK1 mutants. Pharmacological inhibition by kinase inhibitor Compound43 (CP43) has been reported to inhibit TAOK1 and TAOK2 kinases (27). HEK293T cells expressing wild-type sfGFP-TAOK1 were imaged 1 hour after treatment with DMSO or CP43. Whereas TAOK1 distribution was cytosolic in DMSO-treated cells, the presence of kinase inhibitor CP43 led to a robust redistribution of TAOK1 to the plasma membrane (fig. S3A–B). Next, we probed the mechanism through which TAOK1 might localize to the plasma membrane and cause tubulations. We generated several GFP-tagged TAOK1 deletion constructs to map the minimal domain required for its plasma membrane localization (Fig. 3A). When expressed in HEK293T cells, the GFP-tagged kinase domain (residues 1–320) construct was cytosolic, whereas the construct lacking the kinase domain (residues 321–1001) localized to the plasma membrane and led to formation of extensive membrane protrusions (fig. S3C). Further dissection revealed that the C-terminal tail (residues 901–1001) was dispensable, and that residues 321–901 were necessary and sufficient for TAOK1 association with the plasma membrane and for generation of membrane protrusions (Fig. 3B and fig. S3C–D). Cellular fractionation of HEK293T cells expressing GFP-tagged kinase domain (residues 1–320) or coiled-coil domain (residues 321–901), confirmed that the coiled-coil domain was primarily membrane associated whereas the kinase domain was cytosolic (Fig. 3C–D). Live-cell imaging revealed that the membrane protrusions were stable membrane extensions that were actively extending but rarely retracted (fig. S3D). The average length of membrane protrusions in cells expressing the TAOK1 coiled-coil domain increased to 11 μm, whereas the average in control cells expressing TAOK1(1–320) was 2 μm (Fig. 3E). Expression of the membrane-binding domain (residues 321–901) of TAOK1 in neurons led to severe perturbation of neuronal morphology, similar to that exhibited by the NDD mutants (Fig. 3F), whereas constructs expressing the kinase domain or C-terminal tail domains were localized to the cytoplasm and did not perturb neuronal morphology (Fig. 3F–G).

TAOK1 helical bundle directly binds phosphoinositides

To gain structural insight into how the coiled-coil domain of TAOK1 might associate with plasma membrane, we used the machine learning based protein-structure prediction software, AlphaFold2.0 (28, 29). The prediction (AlphaFold ID: Q7L7X3) revealed that the three coiled-coils fold into a triple helix bundle (residues 444–884) that is linked to the kinase domain (residues 1–320) with a long linker which is predicted with low confidence and may be unstructured in isolation (Fig. 4A and fig. S4A–B). We used the Adaptive Poisson-Boltzmann Solver (30) function of Pymol to generate an electrostatic map of surface residues of the predicted triple helix. The triple helix domain formed a gently

curved crescent shaped structure with prominent separation of charged residues. The convex side of the triple helix was positively charged, whereas the concave surface was negatively charged (Fig. 4B). This suggested that the triple helix might directly bind negatively charged lipids in the plasma membrane through electrostatic interactions with the basic amino acids on its convex surface. To test whether the TAOK1 triple helix can directly bind lipids, we bacterially purified GST-tagged TAOK1(321–901) protein (fig. S3E–F) and applied them to the lipid overlay assay. We found that TAOK1 bound phosphatidylinositol (4)-phosphate (PI4P), phosphatidylinositol (4,5)-bisphosphate, and phosphatidylinositol (3,4,5)-triphosphate but did not bind phosphatidylinositol (PI) or phosphatidylethanolamine (PE) (Fig. 4C–D). When transfected in HEK293T cells, the PI(4,5)P2 sensor GFP-C1-PLC∂-PH (31) localized to the plasma membrane as expected. Consistent with the tubulating activity of TAOK1 triple helix bundle, when mCherry-TAOK1(321–901) was co-transfected with the PI(4,5)P2 sensor, we observed the formation of abnormal, long protrusions of the plasma membrane (Fig. 4E). These results collectively show that TAOK1 can directly interact with negatively charged phospholipids enriched in the plasma membrane through its triple helical domain.

Catalytic activity of TAOK1 rescues aberrant plasma membrane association and tubulation

Upon discovering that TAOK1 can directly bind plasma membrane through association with negatively charged phosphoinositides, we investigated why TAOK1 kinase-dead mutants, but not the active kinase, were strongly plasma membrane-bound. One possibility was that the kinase domain autophosphorylates itself to negatively regulate membrane association. To test this hypothesis, we transfected HEK293T cells with either GFP-tagged TAOK1(321–901) alone or coexpressed with mCherry-TAOK1(1–320) kinase domain (Fig. 5A). When expressed alone, the TAOK1 triple helical domain localized to the plasma membrane and led to numerous protrusions; however, co-expression of the kinase domain (residues 1–320) with the triple helical domain rescued both the membrane binding and tubulating effect of the TAOK1 triple helix (Fig. 5A–B). The inactive kinase domain TAOK1 (1–320 K57A) did not rescue the membrane localization of the TAOK1 triple helix. Notably, expression of the isolated kinase domain (residues 1–320) rescued the membrane association of all four catalytically deficient NDD-associated mutants: S111F, L167R, A219V and R269Q (Fig. 5C–D). Further, in the presence of this active kinase domain, the TAOK1 mutants also failed to generate aberrant cellular protrusions (Fig. 5C, D). These results suggest that the kinase activity of TAOK1 inhibits the membrane-binding of the protein's triple helix through the phosphorylation of key residues within the triple helical domain.

Proteomic identification of residues that control TAOK1 membrane association

We hypothesized that TAOK1 induces conformational changes in its helical membrane-binding domain through autophosphorylation, thereby negatively regulating membrane binding and tubulation. To test this, we first used mass spectrometry to identify residues that TAOK1 might phosphorylate in order to regulate its membrane association. GFP-tagged wild-type TAOK1 and kinase-deficient TAOK1 (L167R) were expressed in HEK293T cells and immunoprecipitated using anti-GFP antibodies. After extensive salt washes to remove co-immunoprecipitating proteins, immunoprecipitated TAOK1 was subjected to an in vitro kinase assay to allow for autophosphorylation. Several phosphorylated residues

were identified by mass spectrometry for WT kinase (Fig. 6A–B). TAOK1/2 are known to prefer phosphorylation at threonine residues (32, 33); hence, we focused on the three threonine phosphorylation sites—Thr^{440}, Thr^{443} and Thr^{747}—identified proximal and within the helical bundle (Fig. 6A–B). To test which sites were important for regulation of TAOK1 membrane-binding, we generated phosphomutant constructs that abolished phosphorylation at the identified sites by mutating the threonine to an alanine residue. Mutating sites Thr^{440} and Thr^{443} (T440A and T443A) induced the kinase-active TAOK1 to bind the plasma membrane and generate extensive membrane tubules, whereas no apparent effect was observed for the T747A mutation (Fig. 6C–D). These data indicate that autophosphorylation by TAOK1 at the Thr^{440} and Thr^{443} residues is critical for regulating membrane association and outward protrusions. We hypothesized that, if phosphorylation at residues Thr^{440} and Thr^{443} was sufficient for preventing plasma membrane binding, then overexpression of the active kinase domain would not affect membrane binding by the double mutant. GFP-TAOK1(T440A+T443A) when expressed in HEK293T cells along with the inactive kinase domain localized to the plasma membrane as expected. Further, overexpressing the active kinase domain was unable to prevent the membrane binding of the T440A+T443A double mutant (Fig. 6E–F). These data demonstrate that autophosphorylation at residues Thr^{440} and Thr^{443} together regulate the plasma membrane association of TAOK1. Altogether, these results provide direct evidence for TAOK1-mediated mechanisms for remodeling the plasma membrane in an activity-dependent manner (Fig. 6G).

DISCUSSION

Membrane associating proteins that can sense and/or induce membrane curvature provide a direct mechanism for sculpting neuronal morphology (34–38). Aberrations or dysregulation of plasma membrane remodeling during neuronal differentiation, migration or synaptogenesis can underlie the pathogenesis of neurodevelopmental disorders. In this study, we report that the autism and NDD-associated gene *TAOK1* encodes a plasma membrane sculpting kinase. We show that TAOK1 associates with membrane through direct interaction of its coiled-coil domain with phosphoinositides enriched in the plasma membranes. We provide evidence that this ability to associate with membrane leads to emergence of outward protrusions of the plasma membrane. TAOK1 autophosphorylation controls its plasma membrane binding and tubulation properties. Dysfunction in TAOK1 catalytic activity leads to failure in its disengagement from the plasma membrane causing aberrant neuronal membrane protrusions that perturb neuronal morphology. We characterized four distinct NDD mutations that were clustered in the kinase domain, and show that all four mutations render TAOK1 kinase-dead and result in uncontrolled membrane tubulation. In hippocampal neurons, expression of these TAOK1 mutants cause severe defects in dendritic growth. These findings provide a direct mechanism through which NDD-associated mutations in TAOK1 perturb neuronal development.

Whereas there is only one gene encoding TAO in invertebrates, there are three in vertebrates, encoding TAOK1, TAOK2 and TAOK3. Even though the kinase domain is highly conserved, these three TAO kinases have divergent C-terminal tails that confer each specific and distinct functions. Human brain transcriptomics studies show that among the TAO family, the highest expression during human brain development is observed for *TAOK1* followed

by *TAOK2* and then *TAOK3* (21, 39). Both TAOK1 and TAOK2 are strongly associated with neurodevelopmental disorders (40), and there is data suggesting at least two rare missense mutations in *TAOK3* to be associated with ASD (41, 42). Previously, we identified TAOK2 as a transmembrane kinase that tethers the endoplasmic reticulum to microtubules (43). This study provides the first evidence that TAOK1 binds phosphoinositides in the plasma membrane and generates membrane protrusions. Based on the AlphaFold-predicted structure, the C-terminal domain in TAOK3 folds into a triple helix similar to that of TAOK1, and it is conceivable it also has membrane binding and sculpting properties. The TAOK1 autoregulatory phosphosite Thr^{440} is conserved in TAOK3, but Thr^{443} is a Ser residue in TAOK3 instead. TAOK3 also lacks the unstructured tail region of TAOK1 following the triple helix bundle, which could further provide regulation. It is notable that among the three mammalian TAO kinases, TAOK1 is the most evolutionarily similar to the fly dTao and *C. elegans* kin-18, therefore, it is likely that the fly and worm Tao kinase are also plasma membrane sculpting proteins, a possibility that needs future experimental investigation. For example, loss of Tao in flies induces ectopic synapses resulting in miswired connections that alter behavioral responses (19). This fine-tuning of synaptic connection by Tao kinase during neuronal network development might depend on its ability to remodel the plasma membrane. The Taok1 ortholog in *C. elegans*, kin-18 (44), controls contractility and polarity of the early embryo. Interestingly, kin-18 localizes to the cortex and controls rho localization to the membrane (20). In light of our results, it is plausable that kin-18 directly binds the plasma membrane in embryos and regulates polarity and early embryo contraction in *C. elegans*.

Our results show that the catalytic activity of TAOK1 acts as a functional switch. Whereas catalytically active TAOK1 is cytoplasmic, in its ‘kinase-off’ state TAOK1 binds to and tubulates the plasma membrane. Our data suggest that the endogenous TAOK1 exists in both its “kinase-on” cytoplasmic and “kinase-off” membrane bound states. Although our study has identified key residues in TAOK1 that are autophosphorylated to control this on-off switch, further studies are needed to understand TAOK1 autoregulation and the physiological stimuli during neuronal development that mediate phosphorylation of these residues. Our study has found that ASD-associated mutations in TAOK1 protein that render the kinase catalytically dead cause TAOK1 to be trapped in its “kinase off”, membrane bound state, thereby generating aberrant plasma membrane protrusions. We show that the aberrant protrusions associated with TAOK1 mutants can be rescued by restoring its kinase activity, underscoring the potential for design of small-molecule allosteric kinase activators to rescue the kinase from its membrane-trapped state. In addition to mutations within the kinase domain, we speculate that the many missense and truncation mutations in TAOK1 outside its catalytic domain likely also contribute to neurodevelopmental deficits through a dysfunction in kinase activity-dependent membrane remodeling.

From a structural perspective, TAOK1 provides important future avenues to understand how its membrane binding is regulated. Its predicted structure indicates that surface residues lining the convex side of the triple helix are positively charged. These likely mediate electrostatic interactions with the negatively charged phospholipids in the plasma membrane. Based on the structural prediction, residues Thr^{440} and Thr^{443} lie in the loop connecting the triple helix to the kinase domain where it is plausible for an intramolecular phosphorylation

to occur. Several potential mechanisms for regulating membrane binding could be Thr^{440}/Thr^{443} phosphorylation-induced conformational switch, dimerization or oligomerization as seen in BAR domain proteins, or steric hinderance by the kinase domain in its active versus inactive states. Comparative structural analyses of TAOK1 active and inactive states are needed to obtain further molecular insights into its autoregulation. Our data suggests that TAOK1 can regulate its membrane sculpting function through autophosphorylation, a property that is quite unique to TAOK1 compared to other membrane tubulating proteins such as I-BAR proteins. I-BAR domains from different proteins utilize partially distinct mechanisms to deform the plasma membrane and generate filopodia, and can also create signaling platforms at synapses (7). Whether the plasma membrane-sculpting triple-helix bundle of TAOK1 is structurally and functionally similar to the inverse BAR domain proteins, or if it represents an entirely new class of membrane remodeling proteins remains to be tested. Our results reveal the ASD-associated gene TAOK1 as a membrane-sculpting kinase and provides the neurobiological basis for how TAOK1 dysfunction contributes to neurodevelopmental disorders.

MATERIALS AND METHODS

Cell culture and maintenance

HEK293T were grown in DMEM media (Thermo Fisher, Gibco) with 10% fetal bovine serum (Axenia BioLogix) and 1% Pen-Strep (Invitrogen). Cells were maintained at 5% CO2 and 37˚C and passaged every 3 to 4 days. Primary neurons were obtained from dissociating hippocampi obtained from E18 Sprague-Dawley rat (Envigo). Animals work was performed under University of Washington IACUC approved protocol 4421–01. Rat embryos were trypsin-dissociated, and plated at a density of 150,000 neurons per 18 mm glass coverslips (Fisher) or 450,000 neurons per 35 mm glass-bottom dish (MaTek), which were coated with 0.06 mg/mL poly-D-lysine (Sigma) and 0.0025 mg/mL laminin (Sigma). Plating media containing heat-inactivated 10% fetal bovine serum (HyClone), 0.45% dextrose, 0.11 mg/mL sodium pyruvate, 2 mM glutamine in MEM with Earle's BBS was used. Media was changed 4 hours after seeding neurons into maintenance media consisting of Neurobasal Media (Invitrogen), 2% B27 (Invitrogen), 100 units/mL penicillin and 100 mcg/mL streptomycin and 0.5 mM glutamine. Half of the media was replaced with new maintenance media every 3–4 days. For exogenous gene expression, neurons were transfected with 0.5–1.0μg plasmid DNA per coverslip in a 12-well plate (or 1–2μg DNA/35 mm dish) using Lipofectamine-2000 (Invitrogen) following manufacturer's guide.

Molecular cloning

Full length human TAOK1 was obtained from Transomics Technologies in PCR-XL-Topo plasmid and inserted into sfGFP-C1 (Plasmid #54579, Addgene), using the EcoRI and MfeI sites. The resulting N-terminally sfGFP-tagged TAOK1 construct (sfGFP-TAOK1) was fully sequenced (Genewiz, Azenta Life Sciences) and used as template to generate the ASD associated mutants (Genewiz). All constructs were confirmed by sequencing for accuracy. Domain deletion mutants were subcloned from sfGFP-TAOK1 using restriction enzymes EcoRI and MfeI (New England Biolabs) and assembled using NEBuilder HiFi DNA Assembly-New England BioLabs. Resultant plasmids were verified by sequencing.

GST-TAOK1(321–901) was generated by subcloning from the sfGFP-TAOK1 into the pGEX4T1 vector using restriction enzymes NotI and SalI.

Confocal microscopy

All live and fixed cell imaging was performed on a Nikon Ti2 Eclipse-CSU-X1 confocal spinning disk microscope equipped with four laser lines 405nm, 488nm, 561nm and 670 and the Nikon Elements software. A sCMOS Andor camera was used for image acquisition. The microscope was caged within the OkoLab environmental control setup enabling temperature and CO2 control during live imaging. Imaging was performed using Nikon 1.49 100x, Apo 60X, or 40X oil objectives. All image analyses were done using the open access Fiji software.

Immunofluorescence and western blotting

All cells including neurons were fixed using warm 4% paraformaldehyde with 4% sucrose for 20 min at room temperature, followed by 3 washes with phosphate-buffered saline (PBS). One-hour incubation with blocking buffer (4% Normal donkey serum, 0.2M Glycine (pH 7.4) and 0.1% TritonX-100, in PBS) was followed by overnight incubation with primary antibody at 1:1000 dilution in blocking buffer at 4˚C. After four 5-min washes in PBS, cells were incubated with secondary antibody at 1:1,000 dilution in blocking buffer for 3 hours at room temperature or overnight at 4˚C. Coverslips were washed and then mounted onto microscope glass slides with Fluoromont-G™(EMS). Samples for western blot analysis were treated with NuPAGE™ LDS Sample Buffer (4X) (Invitrogen) with 2-Mercaptoethanol at 5% and subsequently heated for 10 min at 95˚C. Samples were electrophoresed on NuPAGE 4–12% Bis-Tris Polyacrylamide gels (Invitrogen) with NuPAGE MOPS running buffer (Invitrogen). Western blots were transferred to PVDF Membrane Immobilon®-P (Millipore-Sigma) with Transfer buffer (25mM Tris, 192mM Glycine, 20% (v/v) Methanol). Transferred blots were blocked in 5% non-fat dry milk and subjected to primary antibody and HRP conjugated secondary antibody before visualization with Pierce SuperSignal™ West Pico PLUS Chemiluminescent Substrate (Thermo Fisher). Western blot images were obtained using the ChemiDoc Imaging System (Bio-Rad Laboratories). Antibodies used are TAOK1 (Rabbit, Proteintech Cat# 26250–1-AP, RRID:AB_2880446), TAOK1 (Mouse, BD Biosciences Cat# 611368, RRID:AB_398890), GST (Mouse, Thermo Scientific Cat# MA4–004, RRID:AB_10979611), Map2 (Chicken, Abcam Cat# ab5392, RRID:AB_2138153), p-TAOK S181 (Rabbit, R and D Systems Cat# PPS037, RRID:AB_2255678) and GFP (Mouse, Sigma-Aldrich Cat# 11814460001, RRID:AB_390913).

Protein purification

TAOK1 C-terminal amino acids 321–901 were cloned into pGEX4T1 vector and transformed into BL21 E. coli (NEB) to express N-terminally GST-tagged TAOK1(321–901). A 25ml starter culture grown from a single colony overnight was used to inoculate 1L LB media, and grown to an O.D, of 0.6 at 37˚C. Protein expression was induced by IPTG at a final concentration of 0.4mM for 12 hours at 18C. Bacteria were collected by centrifugation for 15min at 6000g, washed with ice cold PBS, and the pellet was resuspended in ice cold lysis buffer (50mM Tris pH 8.0, 5mM EDTA, 150mM NaCl, 20% glycerol, 5mM DTT, Protease Inhibitors (Roche cOmplete and PMSF). Addition of 4mg

lysozyme (Sigma) was followed by 30min incubation with 0.5% TritonX-100 and sonication on ice. Supernatant was collected by centrifugation for 60min at 25,000g, and then incubated with Pierce™ GST Agarose for 1 h. Beads were washed with wash buffer (PBS + 1mM DTT + 0.1% Tween20) followed by wash buffer without detergent. Bound protein was eluted and collected in fractions by glutathione elution buffer at pH 8.0 (50mM Tris pH8.0, 250mM KCl, 1mM DTT, 10% glycerol and 30mM glutathione).

Immunoprecipitation kinase assay

HEK293T cells transfected with N-terminally sfGFP-tagged indicated variants of TAOK1 were lysed with HKT buffer (25mM HEPES pH7.2, 150mM KCl, 1% Triton X-100, 1mM DTT, 1 mM EDTA, Protease Inhibitors (Roche, cOmplete). Lysate was precleared with Pierce™ Protein G Agarose and immunoprecipitated with anti-GFP antibodies (Roche Cat. No. 11814460001) bound on protein G agarose. Beads were washed once with HKT, once for 10 min with HKT with 1M NaCl, and washed once with HK buffer (25mM HEPES pH 7.2, 150mM KCl, 1mM DTT, 1 mM EDTA, Protease Inhibitors (Roche, EDTA-free cOmplete tabTM)). Beads were washed twice with the Kinase Buffer (25mM Tris pH 7.5, 10mM MgCl2, 1mM DTT) prior to the in vitro kinase assay. Kinase assay was then performed by incubating with 0.5mM ATP and Halt™ Protease and Phosphatase Inhibitor Cocktail (Thermo Fisher) for 60min at 30˚C on a shaking heat block. Samples were then subjected to western blot analysis (detailed above) to detect TAOK2 autophosphorylation by rabbit antibody against $pSer^{181}$ (R&D Systems, PPS037).

Lipid overlay assay

Nitrocellulose-immobilized phospholipids (assay strips Cat. p6002; Echelon Biosciences) were blocked by incubation for 60min with 3% fatty-acid free BSA in TBST (137mM NaCl, 2.37mM KCl, 19mM Tris base, 0.1% Tween 20). Incubations were carried out at room temperature. Fresh blocking buffer containing 0.5μg/ml GST-TAOK1(321–901) purified protein was added for 60min incubation with the lipid strips. Lipid strips were washed five times with TBST, and then incubated for 1 hour with a 1:1000 dilution of GST-Tag antibody (MA4–004, Thermo Fisher) in blocking buffer. The membrane was washed 5 times and incubated with a 1:10,000 dilution of horseradish peroxidase-conjugated anti-mouse antibodies in blocking buffer. Bound antibodies were detected by chemiluminescence with the SuperSignal West Pico Chemiluminescent Substrate (ThermoScientific, #34080) and imaged on the ChemiDoc Imager (BioRad).

Proteomics and mass spectrometry

HEK293T cells in confluent 6-well plates were transfected with WT or kinase dead TAOK1 GFP-tagged constructs. After 24 hours, cells were lysed in HKT buffer, immunoprecipitated using 50μl packed Protein G beads bound with anti-GFP antibodies (Roche), and in vitro kinase assay was performed on these samples as described above. To denature the proteins, urea was added to the samples to bring it to final 6M urea concentration followed by addition of TCEP (Tris(2-carboxyethyl) phosphine) to 1mM final concentration. Samples were incubated at room temperature for 30min on a slow thermomixer. CAM (chloroacetamide) was added to a final concentration of 3mM and incubated for 10min with slow mixing. Following alkylation, excess CAM was quenched by adding TCEP and pH

was adjusted to 8.0. Denaturing was followed by on bead proteolytic digestion using LysC (MS grade, Wako JP)) for 2 hours at 37˚C on a thermomixer. Reaction mixture was diluted 3 times to bring down the Urea concentration to <2M with TEAB (Triethylammonium bicarbonate). Further digestion by Trypsin (MS grade, Pierce) was performed overnight at 37˚C on a thermomixer. Digestion was stopped by addition of TFA (to final 1%). Peptide samples were then desalted on C18 StageTips and eluted for Mass spectrometric identification. Peptide samples were separated on an Thermo Easy-nLC1200 (Thermo Fisher Scientific) using 20 cm long fused silica capillary columns (100 μm ID, laser pulled in-house with Sutter P-2000, Novato CA) packed with 3μm 120 Å reversed phase C18 beads (Dr. Maisch, Ammerbuch, DE). Liquid chromatography (LC) solvent A was 0.1% (v/v) aq. acetic acid and LC solvent B was 20% 0.1% (v/v) acetic acid, 80% acetonitrile. The LC gradient was 100 min long with 5−35% B at 300 nL/min. MS data was collected with a Thermo Fisher Fusion Lumos Tribrid mass spectrometer. Data-dependent acquisition with a R=60,000 Orbitrap MS1 and R=30,000 Orbitrap MS2 scans collected with a max inject time of 100 msec and a duty cycle of 2 sec. Data .raw files were analyzed by MaxQuant/Andromeda (Cox et al., 2011) version 1.6.2.6 using protein, peptide and site FDRs of 0.01 and a score minimum of 40 for modified peptides, 0 for unmodified peptides; delta score minimum of 17 for modified peptides, 0 for unmodified peptides. MS/MS spectra were searched against the UniProt human database (updated Jan 2021). MaxQuant search parameters: Variable modifications included Oxidation (M) and Phospho (S/T/Y). Carbamidomethyl (C) was a fixed modification. Max. missed cleavages was 2, enzyme was Trypsin/P and max. charge was 7. The initial search tolerance for FTMS scans was 20 ppm. Label-free quantification (LFQ) of MS intensities from five process replicates/condition were processed with Perseus.

Statistics

Statistics were performed in GraphPad software Prism9.0 with the exception of generalized linear model fitting which was performed using R. A p-value less than 0.05 was deemed significant. All experiments were done in triplicate, and experimental sample size and p values are indicated within the corresponding figure legends.

Database Usage

Developing and adult human brain transcriptomics data was obtained and plotted using HBT database (https://hbatlas.org/). This data was generated using Affymetrix GeneChip Human Exon 1.0 ST Arrays from over 1,340 tissue samples sampled from both hemispheres of postmortem human brains with specimens range from embryonic development to adulthood and are representative of both males and females from multiple ethnicities. Allen Brain Atlas was used to search for *Taok1* mRNA expression in mouse brain (https://mouse.brain-map.org/experiment/show/74819235). RNA-Seq data generated by the Genotype-Tissue Expression (GTEx) project from human brain and protein localization data from immunostained human brain tissue was compiled from Human Protein Atlas (https://www.proteinatlas.org/ENSG00000160551-TAOK1/brain). Structural prediction database AlphaFold2.0 was used for analyzing TAOK1 structure.

Supplementary Material

Refer to Web version on PubMed Central for supplementary material.

ACKNOWLEDGEMENTS AND FUNDING:

We are grateful for funding from the National Institute of Mental Health, grant R01MH121674 (to S.Y.). Mass spectrometry work was supported by instrumentation and funding (to S.-E.O.) provided by the National Institute of General Medicine, grant R01GM129090. The EASY-nLC1200 UHPLC and Thermo Scientific Orbitrap Fusion Lumos Tribrid mass spectrometer were purchased with funding from a National Institutes of Health SIG grant S10OD021502 (to S.-E.O.). Statistical analysis support was provided by James MacDonald through funding provided by the UW Intellectual and Developmental Disabilities Research Center, 5P50HD103524-03. The content is solely the responsibility of the authors and does not necessarily represent the official views of the National Institutes of Health.

REFERENCES AND NOTES

1. Doherty GJ, McMahon HT, Mediation, Modulation, and Consequences of Membrane-Cytoskeleton Interactions. Annu Rev Biophys 37, 65–95 (2008). [PubMed: 18573073]
2. Peter BJ, Kent HM, Mills IG, Vallis Y, Butler PJG, Evans PR, McMahon HT, BAR Domains as Sensors of Membrane Curvature: The Amphiphysin BAR Structure. Science 303, 495–499 (2004). [PubMed: 14645856]
3. Heath RJW, Insall RH, F-BAR domains: multifunctional regulators of membrane curvature. J Cell Sci 121, 1951–1954 (2008). [PubMed: 18525024]
4. Frost A, Perera R, Roux A, Spasov K, Destaing O, Egelman EH, Camilli PD, Unger VM, Structural Basis of Membrane Invagination by F-BAR Domains. Cell 132, 807–817 (2008). [PubMed: 18329367]
5. Frost A, Unger VM, Camilli PD, The BAR Domain Superfamily: Membrane-Molding Macromolecules. Cell 137, 191–196 (2009). [PubMed: 19379681]
6. Henne WM, Kent HM, Ford MGJ, Hegde BG, Daumke O, Butler PJG, Mittal R, Langen R, Evans PR, McMahon HT, Structure and Analysis of FCHo2 F-BAR Domain: A Dimerizing and Membrane Recruitment Module that Effects Membrane Curvature. Structure 15, 839–852 (2007). [PubMed: 17540576]
7. Saarikangas J, Zhao H, Pykäläinen A, Laurinmäki P, Mattila PK, Kinnunen PKJ, Butcher SJ, Lappalainen P, Molecular mechanisms of membrane deformation by I-BAR domain proteins. Curr. Biol 19, 95–107 (2009). [PubMed: 19150238]
8. Mattila PK, Pykäläinen A, Saarikangas J, Paavilainen VO, Vihinen H, Jokitalo E, Lappalainen P, Missing-in-metastasis and IRSp53 deform PI(4,5)P2-rich membranes by an inverse BAR domain–like mechanism. J Cell Biology 176, 953–964 (2007).
9. Zihni C, Mitsopoulos C, Tavares IA, Ridley AJ, Morris JDH, Prostate-derived sterile 20-like kinase 2 (PSK2) regulates apoptotic morphology via C-Jun N-terminal kinase and Rho kinase-1. J. Biol. Chem 281, 7317–7323 (2006). [PubMed: 16407310]
10. Moore TM, Garg R, Johnson C, Coptcoat MJ, Ridley AJ, Morris JD, PSK, a novel STE20-like kinase derived from prostatic carcinoma that activates the c-Jun N-terminal kinase mitogen-activated protein kinase pathway and regulates actin cytoskeletal organization. J. Biol. Chem 275, 4311–4322 (2000). [PubMed: 10660600]
11. Dulovic-Mahlow M, Trinh J, Kandaswamy KK, Braathen GJ, Donato ND, Rahikkala E, Beblo S, Werber M, Krajka V, Busk ØL, Baumann H, Al-Sannaa NA, Hinrichs F, Affan R, Navot N, Balwi MAA, Oprea G, Holla ØL, Weiss MER, Jamra RA, Kahlert A-K, Kishore S, Tveten K, Vos M, Rolfs A, Lohmann K, De Novo Variants in TAOK1 Cause Neurodevelopmental Disorders. Am. J. Hum. Genet 105, 213–220 (2019). [PubMed: 31230721]
12. Hunter JM, Massingham LJ, Manickam K, Bartholomew D, Williamson RK, Schwab JL, Marhabaie M, Siemon A, de los Reyes E, Reshmi SC, Cottrell CE, Wilson RK, Koboldt DC, Mol Case Stud, in press, doi:10.1101/mcs.a006180.

13. van Woerden GM, Bos M, de Konink C, Distel B, Trezza RA, Shur NE, Barañano K, Mahida S, Chassevent A, Schreiber A, Erwin AL, Gripp KW, Rehman F, Brulleman S, McCormack R, de Geus G, Kalsner L, Sorlin A, Bruel A-L, Koolen DA, Gabriel MK, Rossi M, Fitzpatrick DR, Wilkie AOM, Calpena E, Johnson D, Brooks A, van Slegtenhorst M, Fleischer J, Groepper D, Lindstrom K, Innes AM, Goodwin A, Humberson J, Noyes A, Langley KG, Telegrafi A, Blevins A, Hoffman J, Sacoto MJG, Juusola J, Monaghan KG, Punj S, Simon M, Pfundt R, Elgersma Y, Kleefstra T, TAOK1 is associated with neurodevelopmental disorder and essential for neuronal maturation and cortical development. Hum. Mutat (2021), doi:10.1002/humu.24176.

14. Satterstrom FK, Kosmicki JA, Wang J, Breen MS, Rubeis SD, An J-Y, Peng M, Collins R, Grove J, Klei L, Stevens C, Reichert J, Mulhern MS, Artomov M, Gerges S, Sheppard B, Xu X, Bhaduri A, Norman U, Brand H, Schwartz G, Nguyen R, Guerrero EE, Dias C, Consortium AS, iPSYCH-B. Consortium, Betancur C, Cook EH, Gallagher L, Gill M, Sutcliffe JS, Thurm A, Zwick ME, Børglum AD, State MW, Cicek AE, Talkowski ME, Cutler DJ, Devlin B, Sanders SJ, Roeder K, Daly MJ, Buxbaum JD, Large-Scale Exome Sequencing Study Implicates Both Developmental and Functional Changes in the Neurobiology of Autism. Cell 180, 568–584.e23 (2020). [PubMed: 31981491]

15. Yu L, Yang C, Shang N, Ding H, Zhu J, Zhu Y, Tan H, Zhang Y, Paternal De Novo Variant of TAOK1 in a Fetus With Structural Brain Abnormalities. Frontiers Genetics 13, 836853 (2022).

16. Ultanir SK, Yadav S, Hertz NT, Oses-Prieto JA, Claxton S, Burlingame AL, Shokat KM, Jan LY, Jan Y-N, MST3 Kinase Phosphorylates TAO1/2 to Enable Myosin Va Function in Promoting Spine Synapse Development. Neuron 84, 968–982 (2014). [PubMed: 25456499]

17. Poon CLC, Mitchell KA, Kondo S, Cheng LY, Harvey KF, The Hippo Pathway Regulates Neuroblasts and Brain Size in Drosophila melanogaster. Curr Biol 26, 1034–1042 (2016). [PubMed: 26996505]

18. Hu C, Kanellopoulos AK, Richter M, Petersen M, Konietzny A, Tenedini FM, Hoyer N, Cheng L, Poon CLC, Harvey KF, Windhorst S, Parrish JZ, Mikhaylova M, Bagni C, de Anda FC, Soba P, Conserved Tao Kinase Activity Regulates Dendritic Arborization, Cytoskeletal Dynamics, and Sensory Function in Drosophila. J Neurosci 40, 1819–1833 (2020). [PubMed: 31964717]

19. Tenedini FM, González MS, Hu C, Pedersen LH, Petruzzi MM, Spitzweck B, Wang D, Richter M, Petersen M, Szpotowicz E, Schweizer M, Sigrist SJ, de Anda FC, Soba P, Maintenance of cell type-specific connectivity and circuit function requires Tao kinase. Nat Commun 10, 3506 (2019). [PubMed: 31383864]

20. Spiga FM, Prouteau M, Gotta M, The TAO kinase KIN-18 regulates contractility and establishment of polarity in the C. elegans embryo. Dev. Biol 373, 26–38 (2013). [PubMed: 23064028]

21. Kang HJ, Kawasawa YI, Cheng F, Zhu Y, Xu X, Li M, Sousa AMM, Pletikos M, Meyer KA, Sedmak G, Guennel T, Shin Y, Johnson MB, Krsnik Ž, Mayer S, Fertuzinhos S, Umlauf S, Lisgo SN, Vortmeyer A, Weinberger DR, Mane S, Hyde TM, Huttner A, Reimers M, Kleinman JE, Šestan N, Spatio-temporal transcriptome of the human brain. Nature 478, 483–489 (2011). [PubMed: 22031440]

22. Sunkin SM, Ng L, Lau C, Dolbeare T, Gilbert TL, Thompson CL, Hawrylycz M, Dang C, Allen Brain Atlas: an integrated spatio-temporal portal for exploring the central nervous system. Nucleic Acids Res 41, D996–D1008 (2013). [PubMed: 23193282]

23. Sjöstedt E, Zhong W, Fagerberg L, Karlsson M, Mitsios N, Adori C, Oksvold P, Edfors F, Limiszewska A, Hikmet F, Huang J, Du Y, Lin L, Dong Z, Yang L, Liu X, Jiang H, Xu X, Wang J, Yang H, Bolund L, Mardinoglu A, Zhang C, von Feilitzen K, Lindskog C, Pontén F, Luo Y, Hökfelt T, Uhlén M, Mulder J, An atlas of the protein-coding genes in the human, pig, and mouse brain. Science 367 (2020), doi:10.1126/science.aay5947.

24. Consortium EA, Lek M, Karczewski KJ, Minikel EV, Samocha KE, Banks E, Fennell T, O'Donnell-Luria AH, Ware JS, Hill AJ, Cummings BB, Tukiainen T, Birnbaum DP, Kosmicki JA, Duncan LE, Estrada K, Zhao F, Zou J, Pierce-Hoffman E, Berghout J, Cooper DN, Deflaux N, DePristo M, Do R, Flannick J, Fromer M, Gauthier L, Goldstein J, Gupta N, Howrigan D, Kiezun A, Kurki MI, Moonshine AL, Natarajan P, Orozco L, Peloso GM, Poplin R, Rivas MA, Ruano-Rubio V, Rose SA, Ruderfer DM, Shakir K, Stenson PD, Stevens C, Thomas BP, Tiao G, Tusie-Luna MT, Weisburd B, Won H-H, Yu D, Altshuler DM, Ardissino D, Boehnke M, Danesh J, Donnelly S, Elosua R, Florez JC, Gabriel SB, Getz G, Glatt SJ, Hultman CM, Kathiresan S,

Laakso M, McCarroll S, McCarthy MI, McGovern D, McPherson R, Neale BM, Palotie A, Purcell SM, Saleheen D, Scharf JM, Sklar P, Sullivan PF, Tuomilehto J, Tsuang MT, Watkins HC, Wilson JG, Daly MJ, MacArthur DG, Analysis of protein-coding genetic variation in 60,706 humans. Nature 536, 285–291 (2016). [PubMed: 27535533]

25. Zou J, Valiant G, Valiant P, Karczewski K, Chan SO, Samocha K, Lek M, Sunyaev S, Daly M, MacArthur DG, Quantifying unobserved protein-coding variants in human populations provides a roadmap for large-scale sequencing projects. Nat Commun 7, 13293 (2016). [PubMed: 27796292]
26. Byeon S, Werner B, Falter R, Davidsen K, Snyder C, Ong S-E, Yadav S, Biorxiv, in press, doi:10.1101/2022.01.04.474970.
27. Giacomini C, Koo C-Y, Yankova N, Tavares IA, Wray S, Noble W, Hanger DP, Morris JDH, A new TAO kinase inhibitor reduces tau phosphorylation at sites associated with neurodegeneration in human tauopathies. Acta Neuropathol Commun 6, 37–16 (2018). [PubMed: 29730992]
28. Tunyasuvunakool K, Adler J, Wu Z, Green T, Zielinski M, Žídek A, Bridgland A, Cowie A, Meyer C, Laydon A, Velankar S, Kleywegt GJ, Bateman A, Evans R, Pritzel A, Figurnov M, Ronneberger O, Bates R, Kohl SAA, Potapenko A, Ballard AJ, Romera-Paredes B, Nikolov S, Jain R, Clancy E, Reiman D, Petersen S, Senior AW, Kavukcuoglu K, Birney E, Kohli P, Jumper J, Hassabis D, Highly accurate protein structure prediction for the human proteome. Nature 596, 590–596 (2021). [PubMed: 34293799]
29. Jumper J, Evans R, Pritzel A, Green T, Figurnov M, Ronneberger O, Tunyasuvunakool K, Bates R, Žídek A, Potapenko A, Bridgland A, Meyer C, Kohl SAA, Ballard AJ, Cowie A, Romera-Paredes B, Nikolov S, Jain R, Adler J, Back T, Petersen S, Reiman D, Clancy E, Zielinski M, Steinegger M, Pacholska M, Berghammer T, Bodenstein S, Silver D, Vinyals O, Senior AW, Kavukcuoglu K, Kohli P, Hassabis D, Highly accurate protein structure prediction with AlphaFold. Nature, 1–7 (2021).
30. Jurrus E, Engel D, Star K, Monson K, Brandi J, Felberg LE, Brookes DH, Wilson L, Chen J, Liles K, Chun M, Li P, Gohara DW, Dolinsky T, Konecny R, Koes DR, Nielsen JE, Head-Gordon T, Geng W, Krasny R, Wei G-W, Holst MJ, McCammon JA, Baker NA, Improvements to the APBS biomolecular solvation software suite. Protein Sci 27, 112–128 (2018). [PubMed: 28836357]
31. Stauffer TP, Ahn S, Meyer T, Receptor-induced transient reduction in plasma membrane PtdIns(4,5)P2 concentration monitored in living cells. Curr Biol 8, 343–346 (1998). [PubMed: 9512420]
32. Yadav S, Oses-Prieto JA, Peters CJ, Zhou J, Pleasure SJ, Burlingame AL, Jan LY, Jan Y-N, TAOK2 Kinase Mediates PSD95 Stability and Dendritic Spine Maturation through Septin7 Phosphorylation. Neuron 93, 379–393 (2017). [PubMed: 28065648]
33. Miller CJ, Lou HJ, Simpson C, van de Kooij B, Ha BH, Fisher OS, Pirman NL, Boggon TJ, Rinehart J, Yaffe MB, Linding R, Turk BE, Comprehensive profiling of the STE20 kinase family defines features essential for selective substrate targeting and signaling output. Plos Biol 17, e2006540 (2019). [PubMed: 30897078]
34. Dharmalingam E, Haeckel A, Pinyol R, Schwintzer L, Koch D, Kessels MM, Qualmann B, F-BAR proteins of the syndapin family shape the plasma membrane and are crucial for neuromorphogenesis. J Neurosci Official J Soc Neurosci 29, 13315–27 (2009).
35. Chatzi C, Westbrook GL, Revisiting I-BAR Proteins at Central Synapses. Front Neural Circuit 15, 787436 (2021).
36. Guerrier S, Coutinho-Budd J, Sassa T, Gresset A, Jordan NV, Chen K, Jin W-L, Frost A, Polleux F, The F-BAR Domain of srGAP2 Induces Membrane Protrusions Required for Neuronal Migration and Morphogenesis. Cell 138, 990–1004 (2009). [PubMed: 19737524]
37. Coutinho-Budd J, Ghukasyan V, Zylka MJ, Polleux F, The F-BAR domains from srGAP1, srGAP2 and srGAP3 regulate membrane deformation differently. J Cell Sci 125, 3390–3401 (2012). [PubMed: 22467852]
38. Carlson BR, Lloyd KE, Kruszewski A, Kim I-H, Rodriguiz RM, Heindel C, Faytell M, Dudek SM, Wetsel WC, Soderling SH, WRP/srGAP3 facilitates the initiation of spine development by an inverse F-BAR domain, and its loss impairs long-term memory. J Neurosci Official J Soc Neurosci 31, 2447–60 (2011).
39. Miller JA, Ding S-L, Sunkin SM, Smith KA, Ng L, Szafer A, Ebbert A, Riley ZL, Royall JJ, Aiona K, Arnold JM, Bennet C, Bertagnolli D, Brouner K, Butler S, Caldejon S, Carey A, Cuhaciyan

C, Dalley RA, Dee N, Dolbeare TA, Facer BAC, Feng D, Fliss TP, Gee G, Goldy J, Gourley L, Gregor BW, Gu G, Howard RE, Jochim JM, Kuan CL, Lau C, Lee C-K, Lee F, Lemon TA, Lesnar P, McMurray B, Mastan N, Mosqueda N, Naluai-Cecchini T, Ngo N-K, Nyhus J, Oldre A, Olson E, Parente J, Parker PD, Parry SE, Stevens A, Pletikos M, Reding M, Roll K, Sandman D, Sarreal M, Shapouri S, Shapovalova NV, Shen EH, Sjoquist N, Slaughterbeck CR, Smith M, Sodt AJ, Williams D, Zöllei L, Fischl B, Gerstein MB, Geschwind DH, Glass IA, Hawrylycz MJ, Hevner RF, Huang H, Jones AR, Knowles JA, Levitt P, Phillips JW, Sestan N, Wohnoutka P, Dang C, Bernard A, Hohmann JG, Lein ES, Transcriptional landscape of the prenatal human brain. Nature 508, 199–206 (2014). [PubMed: 24695229]

40. Nourbakhsh K, Yadav S, Kinase Signaling in Dendritic Development and Disease. Front Cell Neurosci 15, 624648 (2021). [PubMed: 33642997]
41. Iossifov I, O'Roak BJ, Sanders SJ, Ronemus M, Krumm N, Levy D, Stessman HA, Witherspoon KT, Vives L, Patterson KE, Smith JD, Paeper B, Nickerson DA, Dea J, Dong S, Gonzalez LE, Mandell JD, Mane SM, Murtha MT, Sullivan CA, Walker MF, Waqar Z, Wei L, Willsey AJ, Yamrom B, Lee Y-H, Grabowska E, Dalkic E, Wang Z, Marks S, Andrews P, Leotta A, Kendall J, Hakker I, Rosenbaum J, Ma B, Rodgers L, Troge J, Narzisi G, Yoon S, Schatz MC, Ye K, McCombie WR, Shendure J, Eichler EE, State MW, Wigler M, The contribution of de novo coding mutations to autism spectrum disorder. Nature 515, 216–221 (2014). [PubMed: 25363768]
42. Krumm N, Turner TN, Baker C, Vives L, Mohajeri K, Witherspoon K, Raja A, Coe BP, Stessman HA, He Z-X, Leal SM, Bernier R, Eichler EE, Excess of rare, inherited truncating mutations in autism. Nat Genet 47, 582–588 (2015). [PubMed: 25961944]
43. Nourbakhsh K, Ferreccio AA, Bernard MJ, Yadav S, TAOK2 is an ER-localized kinase that catalyzes the dynamic tethering of ER to microtubules. Dev Cell 56, 3321–3333.e5 (2021). [PubMed: 34879262]
44. Berman KS, Hutchison M, Avery L, Cobb MH, kin-18, a C. elegans protein kinase involved in feeding. Gene 279, 137–147 (2001). [PubMed: 11733138]

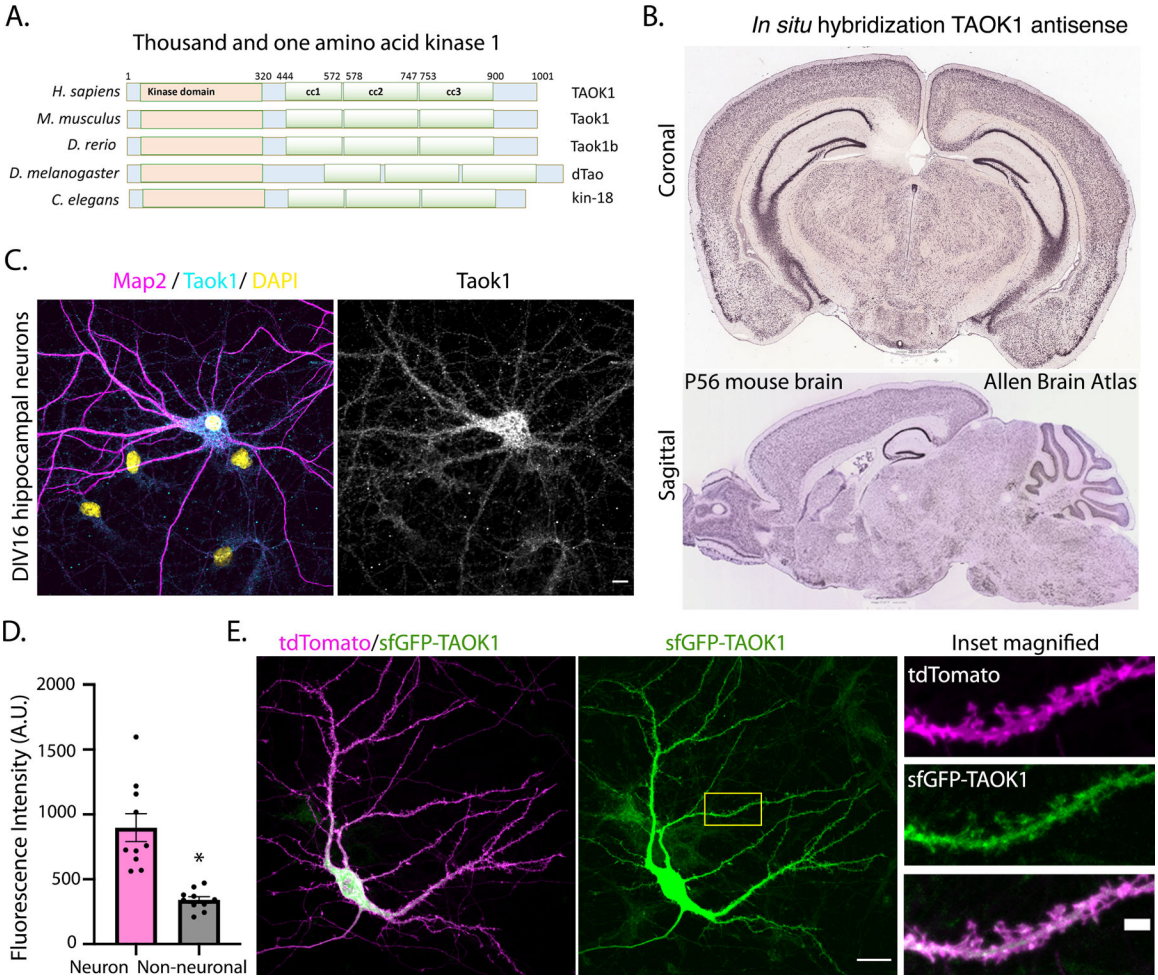

Figure 1. TAOK1 is an evolutionarily conserved serine/threonine kinase that is abundant in hippocampal neurons.

(A) Schematic representation of secondary structure of Thousand and one amino acid kinase 1 orthologs found in human (TAOK1), mouse (Taok1), fish (Taok1b), fly (dTao) and worm (kin-18) species. The N-terminal kinase domain (orange) and three predicted coiled-coils (green) are highly evolutionarily conserved at the sequence and structural level. **(B)** In situ hybridization data from the Allen Brain Atlas using antisense probe against *Taok1* on sagittal and coronal sections of P56 C57BL6/J male mouse brain. **(C)** Primary hippocampal neurons obtained from E15 rat embryos were fixed at 16 days in vitro (DIV) and immunostained using antibodies against Taok1 (cyan) and dendritic protein Map2 (magenta). Nucleus is stained with DAPI (yellow). Grayscale image shows Taok1 immunostaining. Scale bar, 10μm. **(D)** Immunofluorescence intensity of Taok1 in neuronal cells (Map2 positive) compared to non-neuronal cells. Data are means ± SEM from n= 10 cells each, neuronal and non-neuronal. *P= 0.0005 by unpaired t-test with Welch's correction. **(E)** DIV9 hippocampal neurons were transfected with sfGFP-TAOK1 (green) along with cytosolic tdTomato (magenta) and fixed at DIV12 to visualize TAOK1 localization and neuronal morphology. Scale bar, 20μm. Yellow-demarcated section

magnified to assess localization of TAOK1 within dendrites and dendritic spines; scale bar, 2μm.

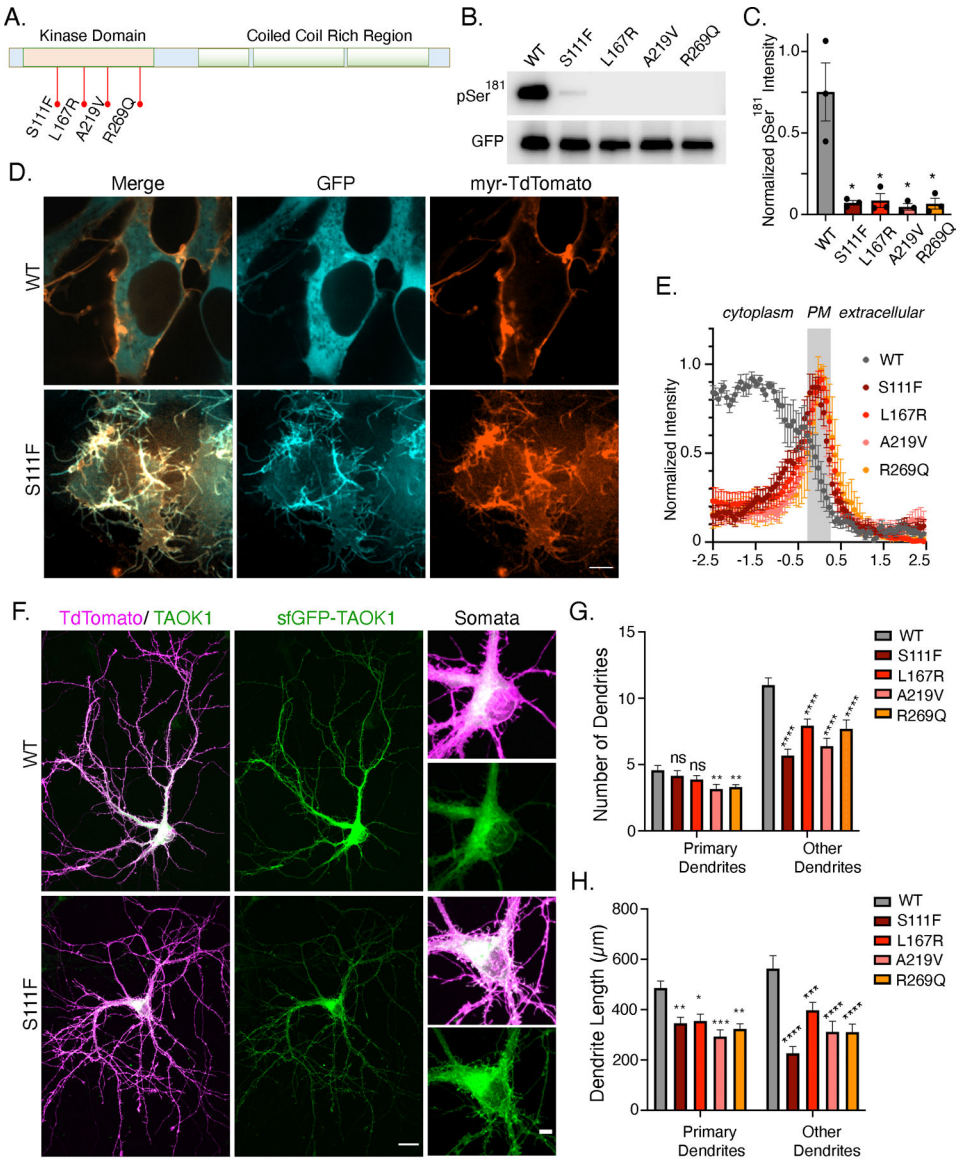

Figure 2. NDD associated mutations that render TAOK1 catalytically dead induce aberrant membrane protrusions and perturb normal dendrite development.

(A) Schematic depicts the secondary protein structure of TAOK1 and marks the position of the four NDD-associated mutations clustered within the N-terminal kinase domain of TAOK1. **(B)** Western blot shows in vitro kinase activity of immunoprecipitated GFP-tagged wildtype (WT) TAOK1 and the four mutants as indicated. Autophosphorylation at residue Ser^{181} is used as a readout for kinase activity and amount of total TAOK1 protein is indicated by GFP blot. (C) Kinase activity as measured by intensity of $pSer^{181}$ signal normalized to the GFP signal is plotted in the bar graph. Mean ±SEM from n=3 experiments. P<0.0001 by one way ANOVA with Dunnett's multiple comparison test. (D) Images show representative HEK293T cells expressing plasma membrane marker myr-tdTomato (red) along with either wild-type TAOK1 (WT) or NDD-associated TAOK1 mutant S111F (cyan). Single confocal plane is shown. Scale bar, 10μm. **(E)** Plot depicts the normalized fluorescence intensity distribution of GFP-TAOK1 wild-type and ASD-

associated mutants S111F, L167R, A219V and R269Q across a 5-μm line across a single z plane of a confocal image, drawn such that 2.5μm is intracellular, 0μm refers to plasma membrane, and the remaining 2.5μm is extracellular. Normalized mean intensity values as a function of distance are plotted and error bars represent SEM from n=6 cells per condition. **(F)** DIV11 rat hippocampal neurons expressing WT-TAOK1 or S111F ASD-associated mutant TAOK1 (green) along with cytoplasmic td-tomato (magenta) to visualize neuronal morphology. Right column shows the magnified somatic region of the neuron to highlight the localization of WT TAOK1 (top) compared to S111F mutant. **(G)** Total number of primary dendrites and secondary or tertiary (others) dendrites in hippocampal neurons expression GFP-tagged WT TAOK1 or the mutants S111F, L167R, A219V and R269Q is plotted. Mean ±SEM from n>14 neurons per condition from 3 different experiments. ns= not significant, ** $p<0.005$, and **** $p<0.0001$ by fitting a generalized linear model with a Poisson link function. **(H)** Total length of primary dendrites and secondary or tertiary (others) dendrites in hippocampal neurons expression GFP-tagged WT TAOK1 or the mutants S111F, L167R, A219V and R269Q is plotted. Mean ±SEM from n>14 neurons per condition from 3 different experiments. ns= not significant, *$p<0.05$, **$p<0.005$, ***$p<0.001$, and **** $p<0.0001$ by 2-way ANOVA with Dunnett's multiple comparisons.

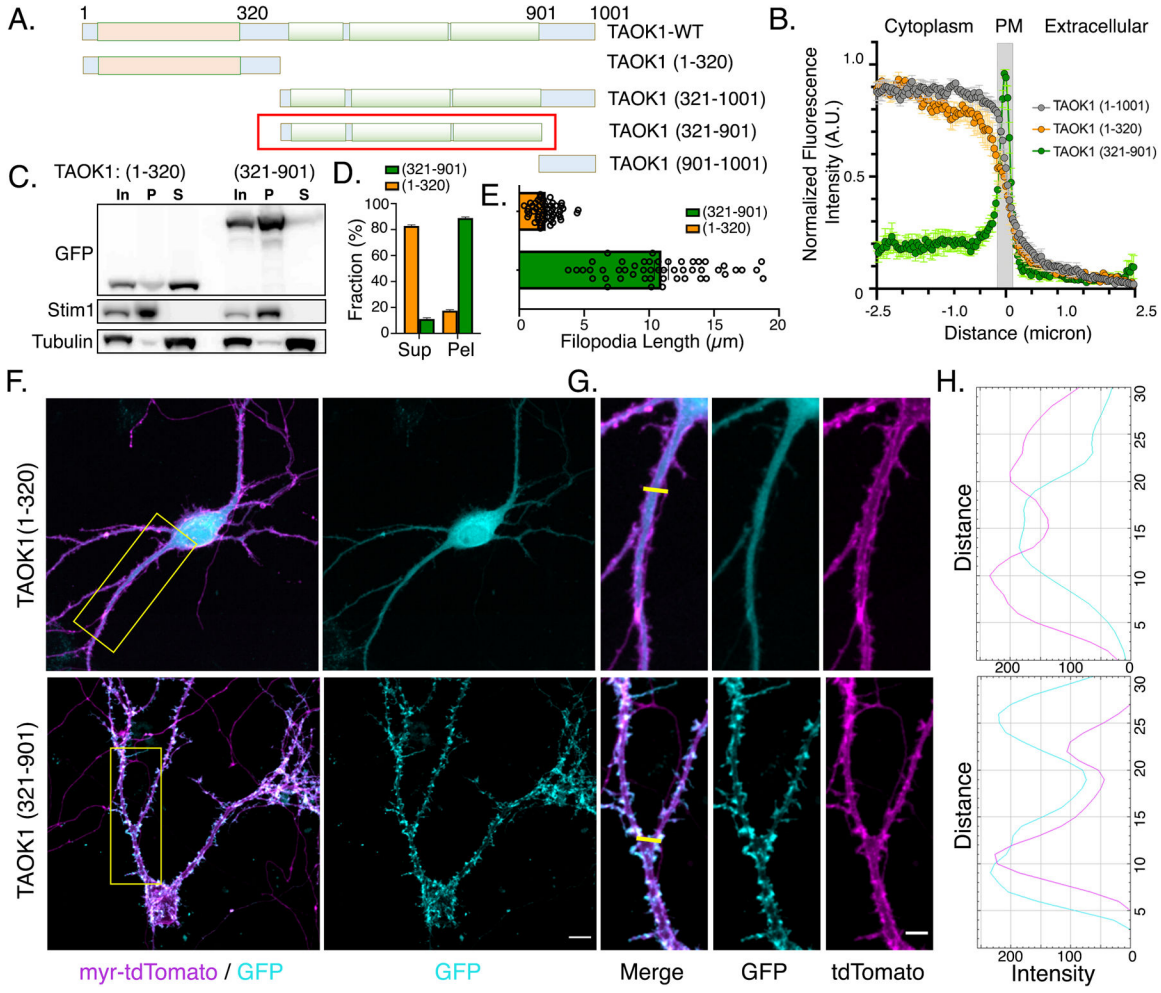

Figure 3. Coiled coil domain of TAOK1 binds and tubulates plasma membrane.

(A) Schematic depicts the different deletion constructs generated to identify the membrane binding domain within TAOK1. The red box indicates the region necessary and sufficient for TAOK1 plasma membrane association. **(B)** Plot depicts the normalized fluorescence intensity distribution of full-length GFP-TAOK1 (1–1001 amino acids), kinase domain (1–320 amino acids) and coiled coil domain (321–901 amino acid) across a 5-μm line across a single z plane of a confocal image of HEK293T cells, drawn such that 2.5μm is intracellular, 0μm refers to plasma membrane and the remaining 2.5μm is extracellular. Normalized mean intensity values are plotted as a function of distance ± SEM from n=10 cells per condition. **(C)** Western blotting for the localization of GFP-tagged TAOK1 kinase domain (1–320) and coiled-coil domain (321–901) in supernatant (S) and membrane pellet (P) fractions, respectively, of HEK293T cells. Fractions were obtained by differential centrifugation at 100,000g. TAOK1 domains were detected by immunoblotting using anti-GFP antibodies. ER protein Stim1 and α-tubulin were controls for the pellet and supernatant fractions, respectively. **(D)** Mean percentage of GFP tagged kinase domain and coiled-coil domain protein present in the pellet and supernatant fractions from (C) is plotted from n=3 experiments. P<0.0001 by 2 way-ANOVA. **(E)** Mean length of plasma membrane protrusions in HEK293T cells expressing either the kinase domain (1–320) or the coiled

coil domain (321–901) is plotted ± SEM, from n=50 protrusions from 10 cells each. P<0.0001 by unpaired t-test with Welch's correction. **(F and G)** DIV11 rat hippocampal neurons expressing GFP-tagged TAOK1 kinase domain (1–320) or coiled coil domain (321–901) (cyan) along with membrane marker myristoylated-tdTomato (magenta) to visualize neuronal morphology (F) and analyze colocalization (G). Yellow box in (F) demarcates the area magnified in (G). Scale bars, 10 and 3 μm, respectively. **(H)** Plot profile of GFP (cyan) and myrTdTomato (magenta) fluorescence shown in (G) as a function of distance in pixels. Data are representative of 3 experiments.

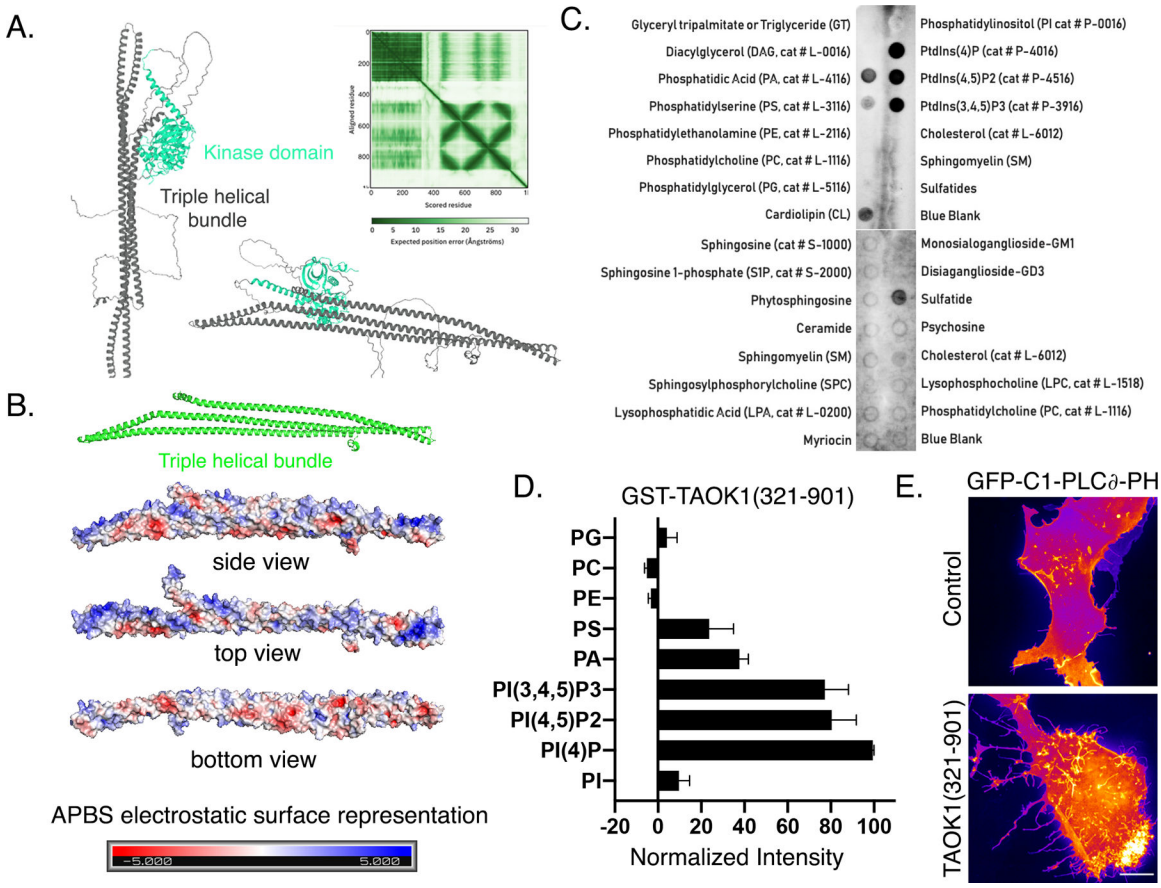

Figure 4. TAOK1 directly associates with phosphoinositides and sculpts the plasma membrane.

(A) AlphaFold2.0 prediction of the structure of human TAOK1. The kinase domain is shown in green (residues 1–320) and the rest of protein is shown in gray (321–1001). The three coiled coil domain (444–901) are predicted to fold into a triple helix. Expected position error at each residue is plotted for the entire length of the protein (top right). The linker region between kinase domain and triple helix (321–443) has a low per-residue confidence score, pLDDT <50. **(B)** The isolated triple helix bundle is shown in neon green. The APBS (Adaptive Poisson-Boltzmann Solver) function of Python was used on the Alphafold2.0 predicted structure of TAOK1 triple helix to create a surface electrostatic representation. The convex face of the crescent shaped protein domain (side view, top view) is highly enriched in positive charges (blue), and the concave side (side view, bottom view) is enriched in negatively charged amino acids (red). The scale of charges -5 to +5 is shown as gradation in shades of red and blue. **(C)** Lipid overlay blots show the binding affinity of a GST-tagged TAOK1 triple helix (321–901) construct to different species of lipids dotted on the blot. Darker dots depict greater binding, detected through antibody against GST tag. **(D)** Quantification of binding affinity of GST-TAOK1(321–901) with different lipids. Mean ±SEM from n=3 experiments. **(E)** Images shows representative HEK293T cells transfected with the PI(4,5)P2 sensor GFP-C1-PLC∂-PH along with either control (top) or mCherry-TAOK1(321–901), assessing for protrusions from the plasma membrane. Scale bar, 5μm.

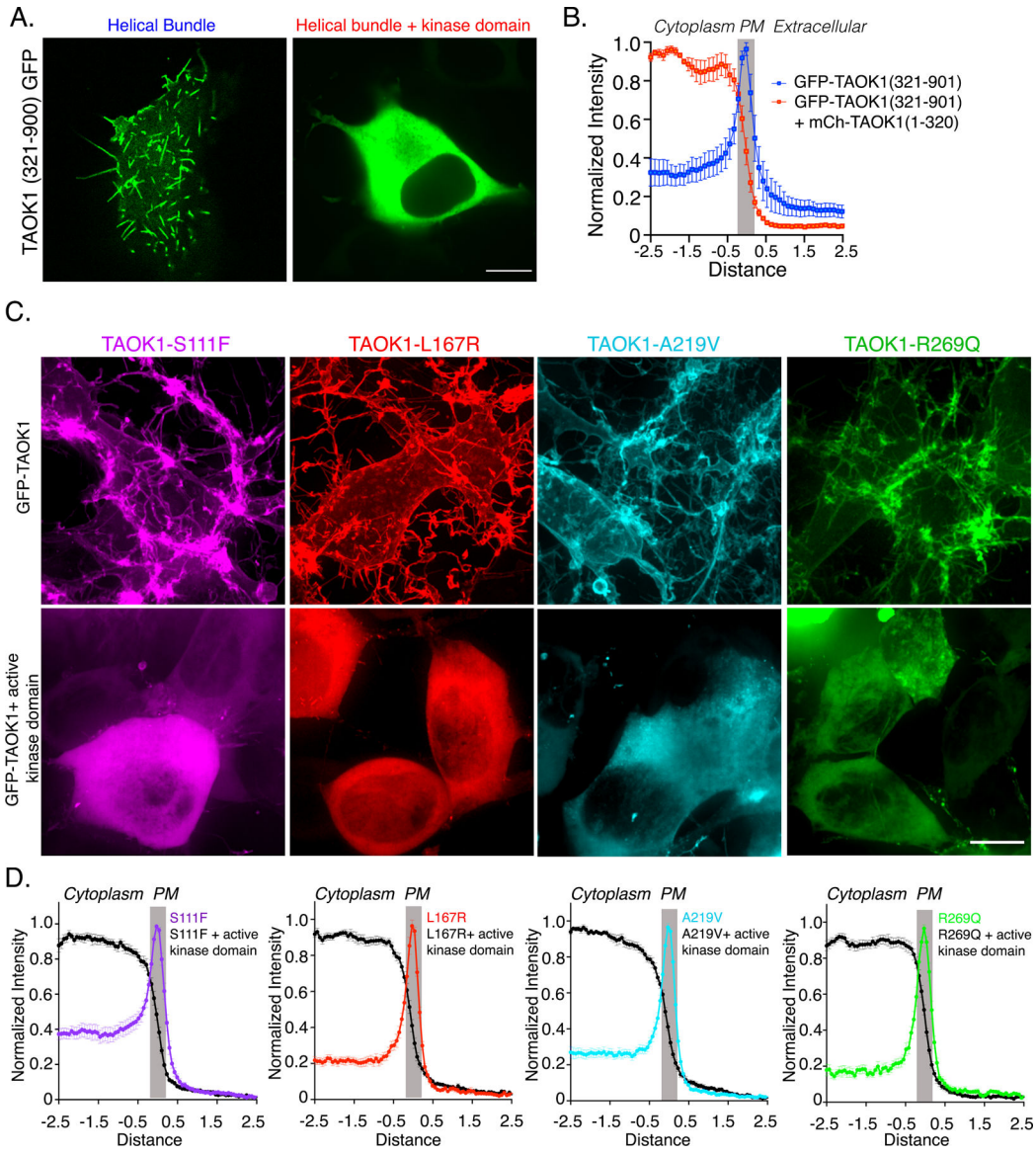

Figure 5. Autophosphorylation rescues aberrant plasma membrane association and tubulation by TAOK1.

(A) HEK293T cells transfected with TAOK1 helical bundle domain GFP-TAOK1 (321–901) alone or with TAOK1 kinase domain mCherry-TAOK1 (1–321). Scale bar, 5μm. **(B)** Plot depicts the normalized fluorescence intensity distribution of the helical bundle domain as in (A), alone (blue) or with the kinase domain (red) across a 5-μm line across a single z plane of a confocal image, drawn such that 2.5μm is intracellular, 0μm refers to plasma membrane, and the remaining 2.5μm is extracellular. Normalized mean intensity values as a function of distance are plotted ±SEM from n=10 cells per condition. **(C)** Representative HEK293T cells expressing NDD-associated TAOK1 mutants S111F (magenta), L167R (red), A219V (cyan) and R269Q (green) are shown in top row, and representative HEK293T cells expressing these mutants along with active kinase domain of TAOK1 (1–320) are shown in the bottom row. Scale bar, 10μm. **(D)** Plot depicts the normalized fluorescence

intensity distribution of TAOK1 mutants in (C), assessed and shown as described in (B), from n=6 cells each per condition.

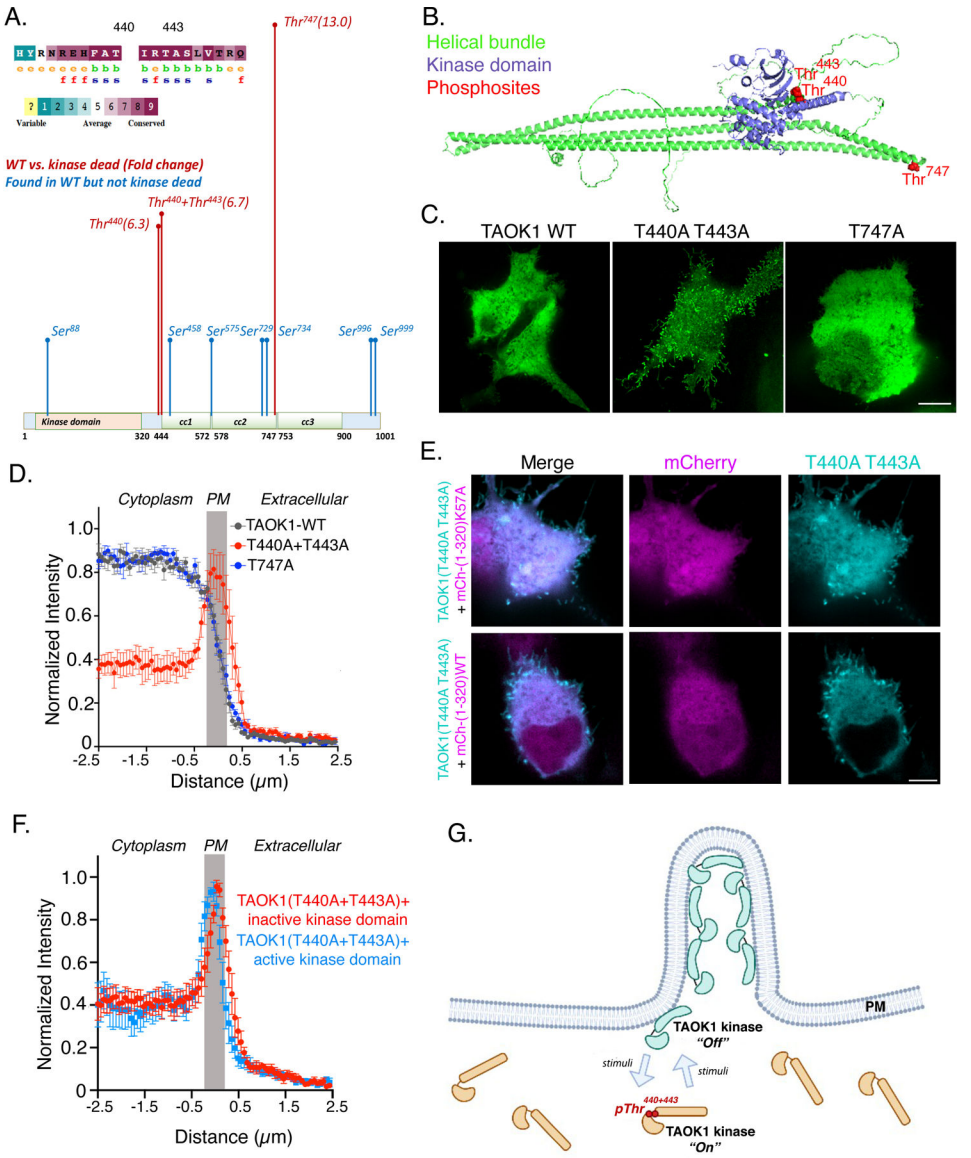

Figure 6. Phosphorylation at residues Thr^{440} and Thr^{443} provide mechanism for autoregulation of TAOK1 membrane association and remodeling function.

(A) Schematics show the phosphorylation sites in TAOK1 identified by mass spectrometry using immunoprecipitated WT TAOK1. Kinase-deficient (L167R) TAOK1 was used as negative control. The fold-change increase in WT over control for the three phosphothreonine sites (red) identified is shown in parenthesis after the phosphosite. The blue, serine phosphorylation sites were only identified in WT TAOK1. Evolutionary conservation of sites was determined using ConSurf. **(B)** Position of the phospho-threonine sites within the predicted 3D structure of TAOK1. Kinase domain is shown in blue, helical bundle in green, and phospho-sites in red. **(C)** Representative confocal images of HEK293T cells transfected with WT TAOK1, double-phosphomutant TAOK1 (T440A+T443A), and phosphomutant TAOK1 (T474A). Scale bar, 10μm. **(D)** Normalized fluorescence intensity distribution of the constructs described in (C) across a 5-μm line across a single z plane of a confocal image, drawn such that 2.5μm is intracellular, 0μm refers to plasma membrane,

and the remaining 2.5μm is extracellular. Normalized mean intensity values as a function of distance are plotted ± SEM, from n=6 cells each per condition. **(E and F)** As described in (C and D) for HEK293T cells transfected with GFP-tagged TAOK1-(T440A+T443A) along with either the active isolated kinase domain mCh-TAOK1-(1–320WT) or the inactive kinase domain mCh-TAOK1-(1–320 K57A), also from n=6 cells each per condition. Scale bar, 5μm. **(G)** Working model of TAOK1 as a membrane-sculpting kinase autoregulated by its kinase activity through phosphorylation at critical residues Thr^{440} and Thr^{443}, which regulates it shuttling between its active cytosolic state (orange) and inactive membrane-bound state (green). NDD-associated mutations (S111F, L167R, A219V and R269Q) render TAOK1 catalytically dead and traps the kinase permanently in the membrane bound state, where it induces aberrant membrane extensions and dendritic defects.